

Stabilities of cable-stiffened cylindrical single-layer latticed shells

Pengcheng Li^{1,2,3a} and Minger Wu^{*1}

¹ Department of Structural Engineering, Tongji University, Shanghai 200092, China

² Key Laboratory of New Technology for Construction of Cities in Mountain Area (Chongqing University),
Ministry of Education, Chongqing 400045, China

³ School of Civil Engineering, Chongqing University, Chongqing 400045, China

(Received November 29, 2016, Revised March 31, 2017, Accepted May 16, 2017)

Abstract. A cable-stiffened cylindrical single-layer latticed shell that is reinforced by cable-stiffened system has superior stability behaviour compared with the ordinary cylindrical latticed shell. The layouts of cable-stiffened system are flexible in this structural system, and different layouts contribute different stiffness to the structure. However, the existed few research primarily focused on the simplest type of cable layouts, in which the grids of the latticed shell are diagonally stiffened by prestressed cables in-plane. This current work examines the stability behaviour of the cable-stiffened cylindrical latticed shells with two different types of cable layouts using nonlinear finite element analysis. A parametric study on the effect of cross-sectional of the cables, pretension in cables, joint stiffness, initial imperfections, load distributions and boundary conditions is presented. The findings are useful for the reference of the designer in using this type of structural system.

Keywords: prestressed cables; latticed shell; stability behaviour; nonlinear analysis; parametric study

1. Introduction

The load-carrying capacity of single layer latticed shell is limited by global instability. However, through the addition of external cable-stiffened system, the load-carrying capacity can be considerably enhanced. The cable-stiffened single layer latticed shell, which was proposed by Schlaich and Schober (1996, 1997), offers an efficient and lightweight structural solution. In this structural system, the grids of the latticed shell are stiffened by prestressed cables that make it flexible enough to apply the cable-stiffened system to any shape of latticed shells. A typical application of this structural system is the Neckarsulm dome (Schlaich and Schober 1996), in which the quadrangular grids are diagonally stiffened in plane by prestressed cables. Additionally, this type of structural system has been adopted in some other practical applications (Umezawa *et al.* 2003).

In addition to the literature describing its practical uses, some research works on cable-stiffened single layer latticed shells have existed since it was developed. Schlaich (Schlaich and Schober 1997) performed an experimental study on the behaviour of this structure based on a practical engineering; Cai *et al.* (2015) conducted a static analysis on a radially retractable hybrid grid shell, he pointed out that the foldable bar shell can be strengthened by the prestressed cables; Zhang and Fujimoto (2010) investigated the buckling behaviour of single layer two-way grid dome with tension member as diagonals, he found that the buckling

load of the dome can be increased from 1.8 to 8.6 times by the prestressed tension member; Bulenda and Knippers (2001) discussed the stability of cable-stiffened grid shells by geometrically nonlinear finite element (FE) analysis, and the importance to select proper imperfections to capture the real load-carrying capacity was presented; Feng *et al.* (2012, 2013) proposed the formulas to evaluate the linear buckling load of cable-stiffened cylindrical and elliptic paraboloid latticed shells, the effect of geometric imperfections was taken into account in the formulas; Li *et al.* (2014) analyzed the stability of cable-stiffened single-layer latticed shells with different types of joints and different layouts of cables.

To the knowledge of the authors, research works on cylindrical cable-stiffened latticed shells have not been attempted except the research completed by Zhang (Zhang and Fujimoto 2010), Cai *et al.* (2013) and Feng *et al.* (2013). And the few existed works on cylindrical cable-stiffened latticed shells were primarily focused on the simplest cable-stiffened system, namely the grids of the latticed shell are diagonally stiffened in-plane by cables. In fact, there are different types of layouts for the cable-stiffened system (Umezawa *et al.* 2003, Li *et al.* 2014), which have been reported to affect the stability of the latticed shell significantly. Besides, research on the effects of joint stiffness to the stability of cable-stiffened cylindrical latticed shell have not been conducted at all as far as the authors are aware, though it has been reported to affect the stability of the ordinary latticed shell (Kato *et al.* 1994, Ramalingam and Jayachandran 2015, López *et al.* 2006, Wen *et al.* 2011, Han *et al.* 2016). This current work investigates the buckling behaviour of cable-stiffened cylindrical latticed shell with two different types of cable layouts. In addition, the effects of cable cross-sectional

*Corresponding author, Ph.D., Professor,
E-mail: wuminger@tongji.edu.cn

^a Lecturer, E-mail: lipengcheng@cqu.edu.cn

area, pretension in cables, joint stiffness, initial imperfections, load distributions and boundary conditions have also been studied in this current study. The commercial code ANSYS (2013) was adopted to complete the FE analyses.

2. Analytical model

As stated earlier, the cable-stiffened cylindrical latticed shell comprises an ordinary cylindrical latticed shell and the cable-stiffened system. In this current research, two types of cable-stiffened systems were adopted to form the stiffened latticed shells. Thus, both the ordinary latticed cylindrical shell and two types of cable-stiffened ones were investigated in this article to compare their stability behaviors.

2.1 Geometrical model

2.1.1 Ordinary cylindrical latticed shell

The geometry principle of the cylindrical latticed shell is shown in Fig. 1, in which the symbols R , H , B and L denote to the radius of the curvature, the height of the shell, the span and the length of the shell. In this investigation, R and H take values 30000 mm and 12000 mm, respectively, and B and L are adopted as 48000 mm and 72000 mm.

The circular edge is divided into 16 members equally, with a length of 3475 mm for each member. The members along the straight edges have the equal length of 3600 mm. Tubular sections are adopted here for all the members of the latticed shell, the out diameters of the members along the straight edges and the circular edges are 325 mm and 203 mm respectively, and the corresponding thicknesses are 8 mm and 6 mm.

2.1.2 Cable-stiffened system

Two different types of cable-stiffened systems, which are adopted to strengthen the ordinary latticed shell, are shown in Fig. 2. In layout I, the cables are used to connect the diagonal joints of the grids. In contrast with layout I, the cable-stiffened system of layout II consists of posts and cables. In this study, a post with a length of 750 mm and a

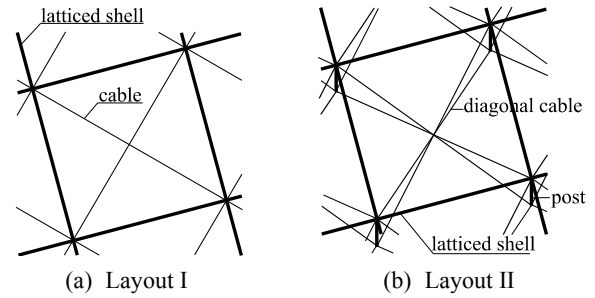


Fig. 2 Different layouts of the cable-stiffened system in the grids

cross-sectional area of 2000 mm², is attached to each joint of the grids, and the diagonal cables are used to connect the ends of the posts and the joints at diagonal corners. Note that all the cables are not connected with each other in the middle of the grids. For convenience, the cable-stiffened single-layer latticed shells with cable layout I, layout II are represented by “Shell I”, “Shell II” respectively. The corresponding single-layer latticed shell without the cable-stiffened system is represented by “Shell”.

2.2 Material properties and element types

The material of the posts and all the members is Q345 steel with a yielding stress of 345 MPa. The corresponding Young’s modulus and Poisson’s ratio are 2.06×10^{11} Pa and 0.3, respectively. The material of the cables is steel spiral strand rope with a Young’s modulus of 1.6×10^{11} Pa. Fig. 3 shows the stress-strain relationships of the steel and cable, in which σ and ϵ denote the stress and strain, respectively. In this study, the steel is assumed to be an ideal elastoplastic material (see Fig. 3(a)); however, the cables are treated as elastic in the analysis (see Fig. 3(b)). It should be noted that the cables in the latticed shells would slack if the strain convert to be compressive.

The quadratic three-node beam element based on Timoshenko beam theory is adopted to simulate the members of the latticed shells. 3-D uniaxial tension-compression spar element is selected to simulate the posts in the FE analyses. In contrast, 3-D uniaxial tension-only spar element is used to simulate the slack of the cables.

2.3 Load and boundary conditions

In this current study, uniformly distributed load was applied to each node of the latticed shells to conduct the analyses with the exception of Section 4.5, in which the

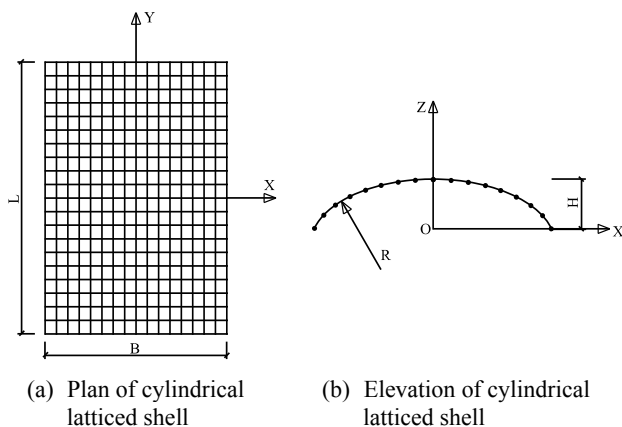


Fig. 1 Geometry principle of single-layer cylindrical latticed shell

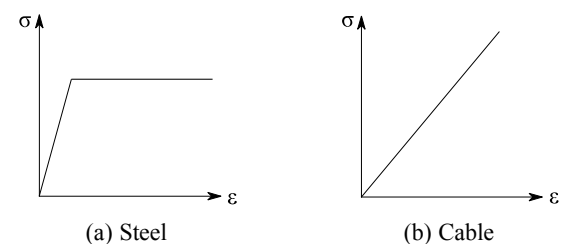


Fig. 3 Stress-strain relationships of the steel and cable

effects of different load distributions were discussed. Similarly, the latticed shells were pin-supported on the four edges except for Section 4.6, in which the effects of boundary conditions were investigated.

3. Methodology

3.1 Procedure

This current work was completed by the following procedure:

Firstly, the linear buckling analysis based on the original configuration of the structure was conducted to obtain the critical loads and buckling modes. Though the critical load is not the real load-carrying capacity due to the imperfection and the nonlinearity of the structure, it can be used to understand the buckling behaviour as an overall estimation. The buckling mode obtained from linear buckling analysis was adopted to simulate the imperfection distribution in the nonlinear analysis.

Subsequently, nonlinear buckling analyses were conducted to capture the real load-carrying capacities of the latticed shells. It should be noted that the geometrical imperfection must be taken into account in the nonlinear analyses. In consistent with the Chinese technical specification for space frame structures (2010) and Eurocode 3 (EN 1993-1-6 2007), most of the previous research works adopted the lowest buckling mode to be the imperfection distribution (Mohammadi *et al.* 2012, Yamashita and Kato 2001). However, it has been reported that the imperfection distribution follows the lowest buckling mode cannot always capture the real load-carrying capacity (Jiang *et al.* 2013). In other words, the governing imperfection distribution, which corresponds to the real load-carrying capacity, does not always follow the lowest buckling mode. Thus, the method to determine the governing imperfection distribution shape becomes part of the work of this article, and it will be discussed in next section. After obtaining the method to determine the governing imperfection distribution shape, parametric studies have also been conducted in this article to investigate the effects of different parameters on the stability behaviors of the latticed shells. In this current work, the pretension is introduced by defining initial strain in cables.

3.2 Imperfection distribution

3.2.1 Linear analysis

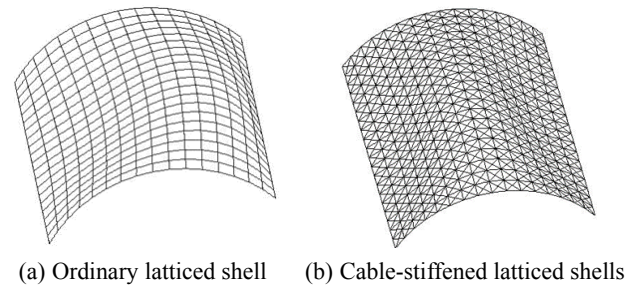


Fig. 4 Buckling modes of cylindrical latticed shell

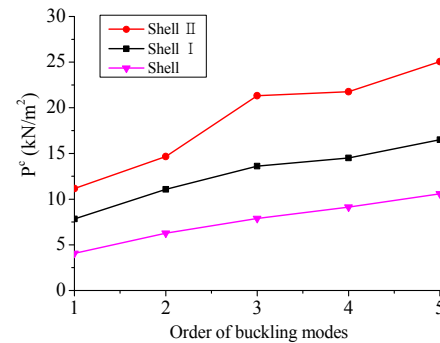


Fig. 5 Critical loads of different types of cylindrical latticed shell

Fig. 4 shows the first buckling modes of ordinary single layer cylindrical latticed shell and cable-stiffened ones with the cable cross-sectional area of 355.98 mm² and the cable pretension of 300 MPa. It must be noted that Fig. 4(b) adopted the buckling mode of Shell I to illustrate the buckling modes of Shell I and Shell II, because the buckling modes of these two cable-stiffened latticed shells exhibit the same buckling mode. As it can be seen, the front elevation of the buckling mode is changed from two half waves to three halfwaves with the introduction of the cable-stiffened systems, implying that the stiffness of the ordinary latticed shell is improved by the cable-stiffened systems.

Fig. 5 shows the critical loads P^c of the single layer cylindrical latticed shells with the same cable cross-sectional area and pretension level as Fig. 4. Obviously, the critical loads have been improved significantly by the cable-stiffened system. In order to investigate the linear buckling loads more accurately, the authors also conducted linear buckling analysis of cable-stiffened latticed shells with different pretensions (see Table 1). Obviously, the buckling loads are much influenced by the pretensions in cables,

Table 1 Linear buckling loads of cable-stiffened latticed shells with different pretensions

| Buckling order | 100 MPa | | 200 MPa | | 300 MPa | | 400 MPa | |
|----------------|---------|----------|---------|----------|---------|----------|---------|----------|
| | Shell I | Shell II |
| 1 | 7.445 | 9.999 | 7.680 | 10.375 | 7.875 | 11.466 | 8.125 | 12.722 |
| 2 | 10.936 | 13.801 | 11.044 | 14.090 | 11.071 | 15.064 | 11.096 | 16.245 |
| 3 | 13.261 | 17.005 | 13.450 | 18.982 | 13.643 | 21.697 | 13.817 | 22.212 |
| 4 | 13.609 | 19.003 | 14.111 | 20.499 | 14.593 | 22.289 | 15.528 | 23.462 |
| 5 | 13.80 | 19.304 | 16.519 | 21.814 | 16.492 | 25.385 | 16.460 | 26.444 |

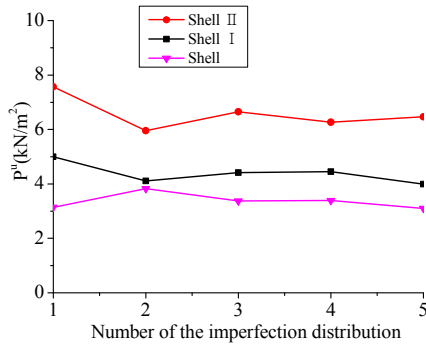


Fig. 6 Load-carrying capacities with different imperfection distributions

especially for Shell II. This is reasonable because the additional stiffness of the cable-stiffened latticed shell results from the existed pretension in cables.

3.2.2 Nonlinear analysis

As mentioned before, this section aims to determine the governing imperfection distribution in order to capture the real load-carrying capacities of the latticed shells. In this current study, the following method is introduced to determine the governing imperfection distribution: The first five buckling modes were adopted to introduce the imperfection distribution in the nonlinear analyses separately, and the one corresponds to the lowest buckling load (real load-carrying capacity) is treated as the governing imperfection distribution.

Fig. 6 shows the load-carrying capacities of the cylindrical latticed shells with different imperfection distributions, which follow the first five linear buckling modes. Thus, the number of the imperfection distribution in Fig. 6 corresponds to the order of the buckling modes in Fig. 5. Both the ordinary latticed shell and the cable-stiffened ones with the cable cross-sectional area of 355.98 mm² and the pretension level of 300 MPa were analyzed in this section. As it can be seen, the governing imperfection distribution corresponds to the real load-carrying capacity of Shell and Shell I follows the 5th buckling mode, however, the governing imperfection distribution of Shell II follows the 2nd buckling mode. In other words, the governing imperfection distribution is not always corresponding to the lowest buckling mode, this conclusion is in line with the previous studies (Jiang *et al.* 2013). However,

it can be found that the governing imperfection distribution of all the latticed shells is antisymmetric buckling mode as shown in Fig. 7. Thus, the subsequent analysis adopted the antisymmetric buckling mode (see Fig. 7) as the initial imperfection distribution. It should be noted that Fig. 7 adopted the antisymmetric buckling mode of Shell I to illustrate the governing imperfection distribution of all the latticed shells, because the governing imperfection distribution of these latticed shells are the same. As for the amplitude of imperfection, $B/300$ (B is the span of the latticed shell) is generally adopted except in Section 4.4.

4. Numerical results

This section discusses the effects of different parameters to the load-carrying capacities of single layer latticed shells using FE analyses. In the FE analyses, the pretension in cables varied from 100 MPa to 400 MPa with a variety of cable cross-sectional area from 116.24 mm² to 464.95 mm². The cross-sectional area of 355.98 mm² and pretension level of 300 MPa with the imperfection magnitude of $B/300$ (B is the span of the latticed shell) are generally selected in the parametric analyses.

4.1 The effect of cross-sectional area of the cables

To investigate the effect of cross-sectional area of the cables, the pretension in cables was fixed at 300 MPa while the cross-sectional area varied from 116.24 mm² to 464.95 mm². Fig. 8 shows the equilibrium paths represented by the load P versus the displacement δ with the cross-sectional area of the cables varying. It must be noted that the displacement depicted in the equilibrium paths in this article is the maximum node deflection of the latticed shell when the instability occurs. As it can be seen, both the stiffness and the load-carrying capacity of the single layer latticed shell have been improved significantly with the introduction of the cable-stiffened system. Similar results can be observed from Fig. 9, which shows the load-carrying capacities of different types of single layer latticed shells. Obviously, the load capacities of Shell I and Shell II are higher than those of shell due to the introduction of the cable-stiffened system. It must be noted that the load-carrying capacity of Shell II is higher than those of Shell I, this can be explained from the different layouts of Shell I and Shell II. As it shown in Fig. 2, the shear stiffness in-

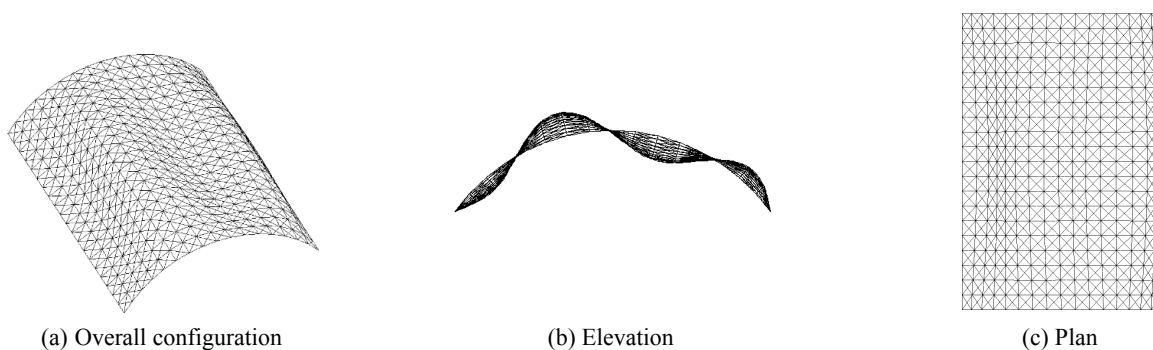


Fig. 7 Governing imperfection distribution

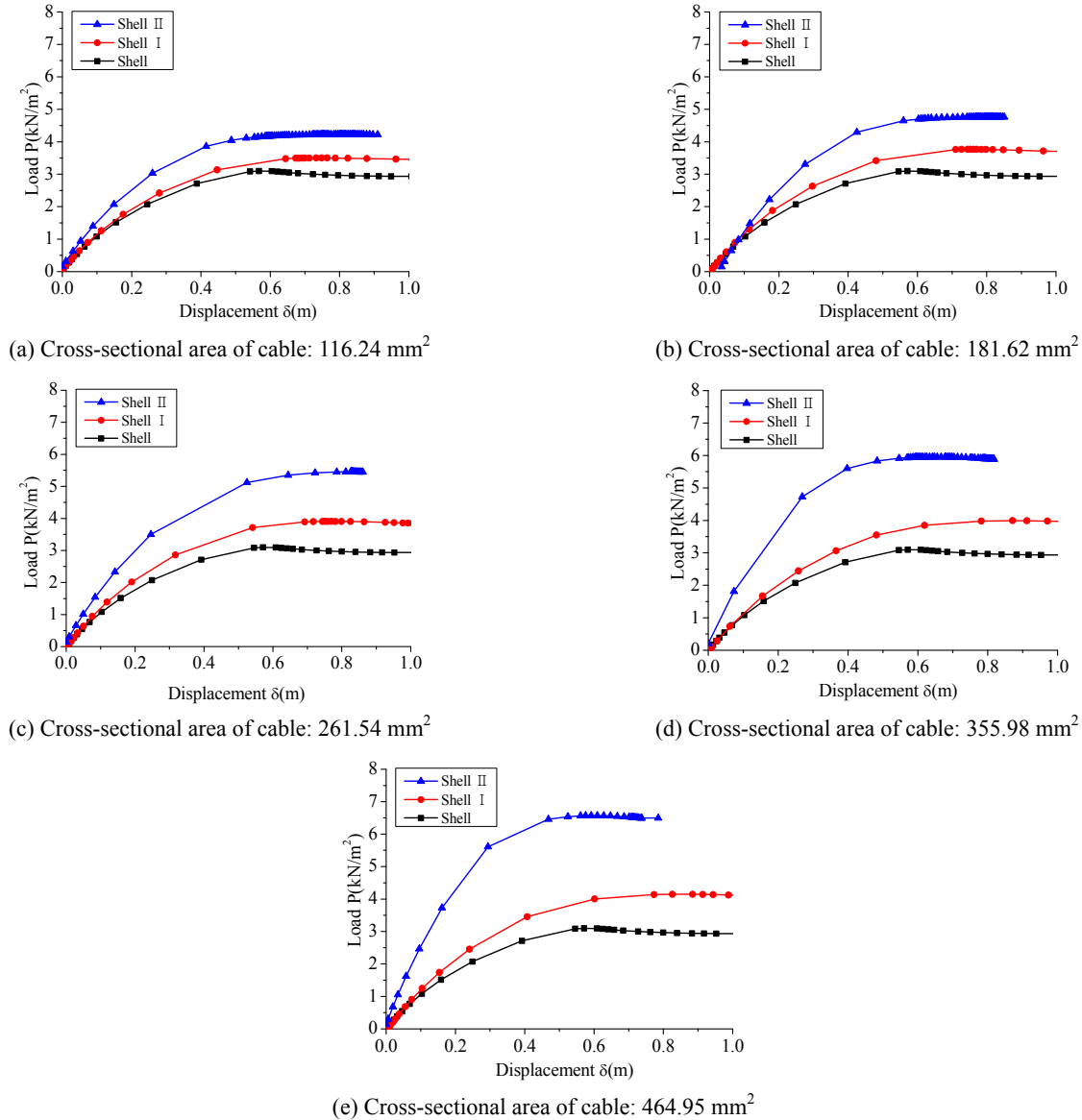


Fig. 8 Equilibrium paths with the cross-sectional area of the cables varying

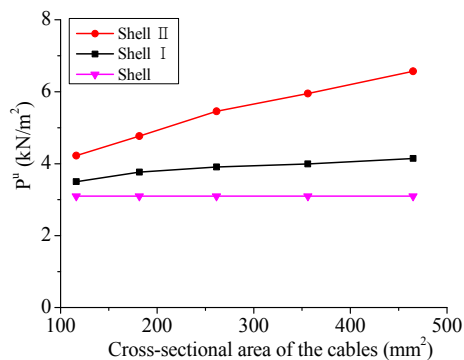


Fig. 9 Load-carrying capacities with the cross-sectional area of the cables varying

plane of the ordinary latticed shell can be improved by the prestressed cables (Shell I); in contrast, both the shear stiffness in-plane and bending stiffness out-of-plane can be improved by the prestressed cables and posts (Shell II).

4.2 The effect of pretension in the cables

In order to investigate the effect of the pretension in the cables, the cross-sectional area of the cables was fixed to 355.98 mm² while the pretension varied from 100 MPa to 400 MPa. Figs. 10 and 11 show the equilibrium paths and the load-carrying capacities of cylindrical latticed shells with different pretension levels in cables. As it can be seen, the load-carrying capacity of Shell I is increased by the pretension slightly, while the load-carrying capacity of Shell II is improved considerably. This can be explained from the different layouts of cable-stiffened systems as well. Both the shear stiffness in-plane and bending stiffness out-plane have been reinforced in Shell II, which means the increase of pretension improve the shear stiffness in-plane and bending stiffness out-plane simultaneously for Shell II. The expressions of the shear and bending stiffness of the grids have been derived by Wu (Wu and Wu 2012).

4.3 The effect of joint stiffness

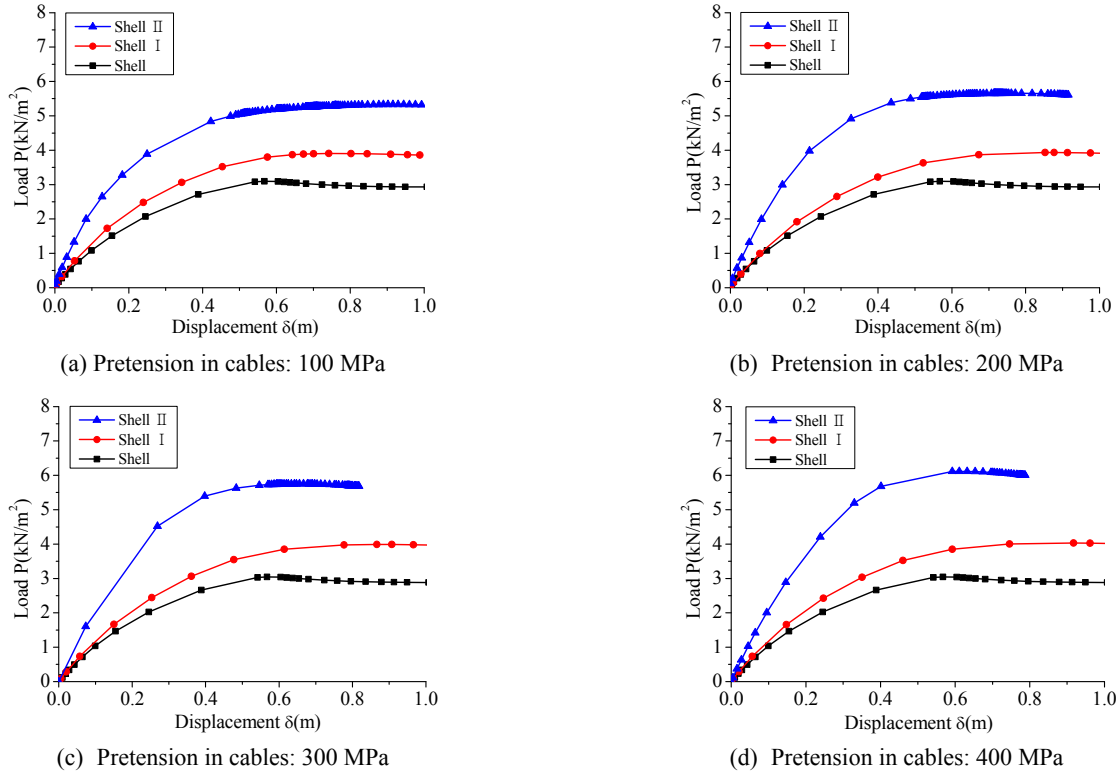


Fig. 10 Equilibrium paths with the cross-sectional area of the cables varying

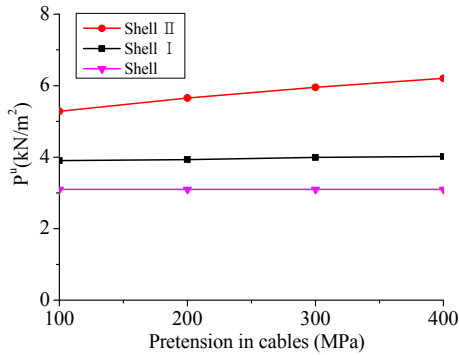


Fig. 11 Load-carrying capacities with the pretension levels in the cables varying

In this section, three different types of joints (rigid joint, semi-rigid joint and scissor joint) are analysed to investigate

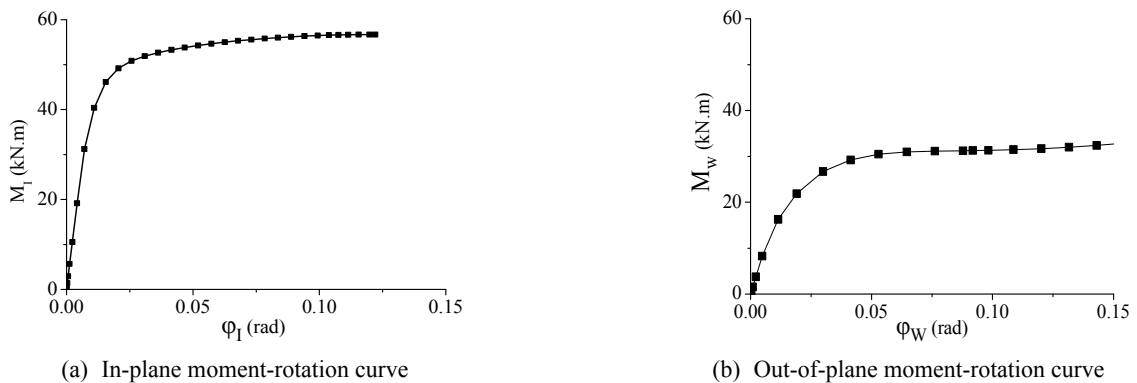


Fig. 12 The curve of the bending moment to rotation of the joint

the effect of joint stiffness on the stability behaviour of both the ordinary cylindrical latticed shell and the cable-stiffened ones. This current work adopted the same method with Li *et al.* (2014) to analyse the effect of joint stiffness. The analytical models of semi-rigid type joint and scissor-type joint are introduced simply in this section, more details about these two types of joints can be found in previous work (Li *et al.* 2014).

4.3.1 Semi-rigid type joint

The members of the latticed shell are connected by unstiffened tubular X-joints, in which the brace members are welded onto the outer surface of the chord members. In accurate analysis, the joint should be taken as semi-rigid due to the deformation of the surface of the chord members. In this study, the in-plane and out-of-plane rotational stiffness of the joints were treated as semi-rigid, the axial and twisting stiffness were taken as rigid. The correspon-

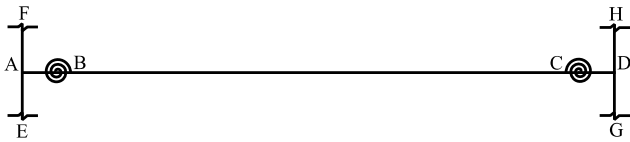


Fig. 13 The semi-rigid model of the brace member

ding moment-rotation relationships which are shown in Fig. 12 are used to simulate the semi-rigid behaviour of the joint. φ_I is the in-plane rotation of the joint, and φ_w is the out-of-plane rotation of the joint; M_I and M_w are the corresponding moment of the joint respectively. The methodology to obtain the moment-rotation relationship was explained by Li *et al.* (2014).

Fig. 13 shows the simplified model of the semi-rigid tubular joint for the buckling analysis of the shells. EF and GH are the chord members, while AD is the brace members. AB and CD are the intersection zones, with the length of the radius of the chord member and the material properties of the brace member. Two nonlinear spring elements are selected to simulate the semi-rigid properties of the tubular

joint in-plane and out-plane, the rotational stiffness of the spring elements is described according to the corresponding moment-rotation relationship shown in Fig. 12. The spring elements are set at the outer surface of the chord members, which are represented by B and C in Fig. 13.

4.3.2 Scissor-type joint

The detail of the scissor-type joint is shown in Fig. 14, two members of the latticed shell are connected by the pin at the intersection. Obviously, these two members can rotate freely in-plane due to the characteristic of the pin. In this analysis, the combin7 element in ANSYS (2013) was used to simulate the scissor-type joint.

Fig. 15 shows the equilibrium paths with different joint types. It can be seen from Fig. 15 that the load-carrying capacity of ordinary latticed shell is decreasing with the decrease of joint stiffness, especially when the joint is scissor joint. However, the effect of these three different types of joints on the load-carrying capacities of cable-stiffened latticed shells is negligible, this characteristic make it possible to apply scissor joint to the cable-stiffened latticed shells.

4.4 The effect of geometrical imperfections

Based on the previous study (Yamada *et al.* 2001, Zugasti *et al.* 2012), the load-carrying capacity of the single layer latticed shell is sensitive to imperfections. In this study, the amplitude of the geometrical imperfection varied from B/10000 to B/100, where B represents the span of the latticed shell. As mentioned before, the method introduced in Section 3.2 was adopted to determine the imperfection distribution shapes.

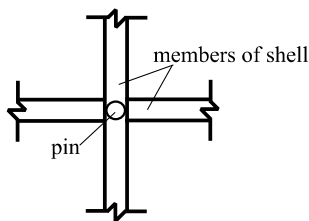


Fig. 14 Detail of the scissor-type joint

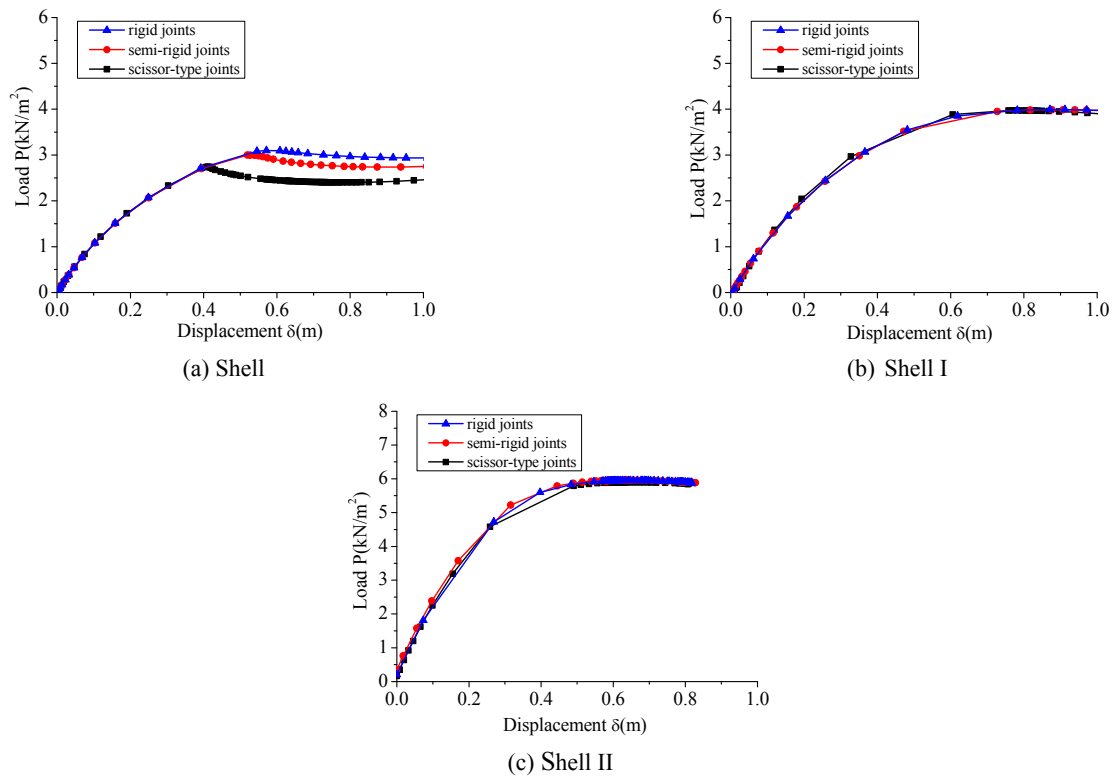


Fig. 15 Equilibrium paths with different joint types

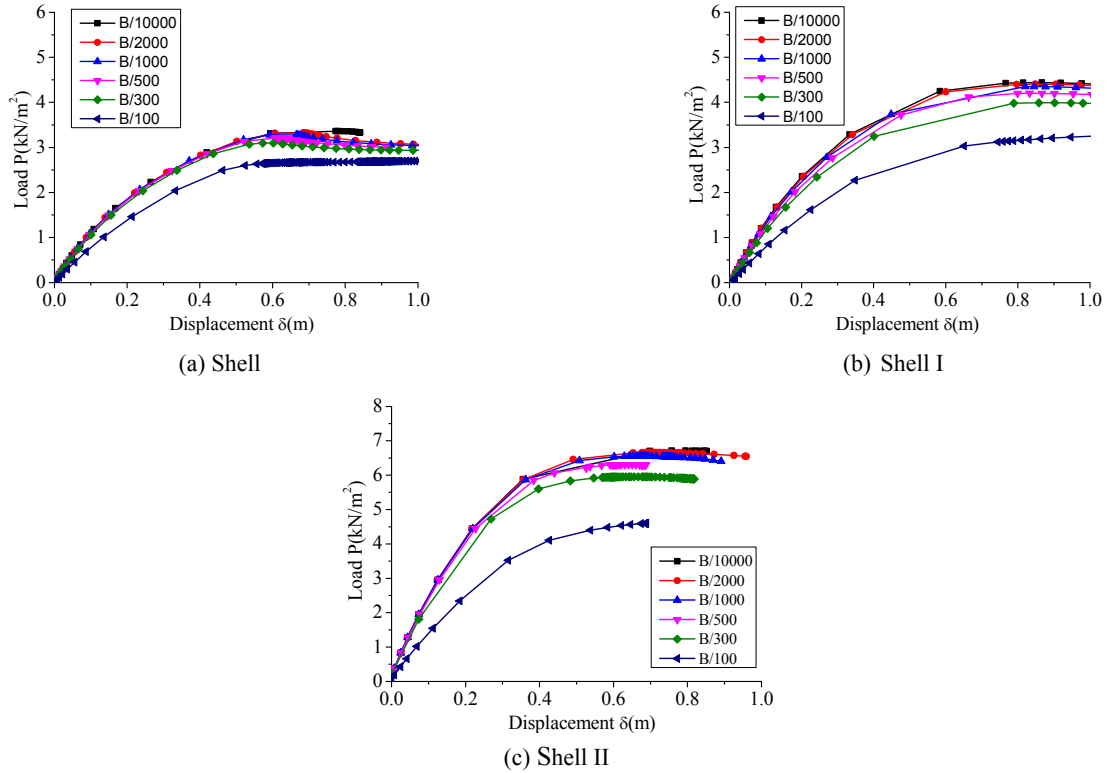


Fig. 16 Equilibrium paths with different amplitudes of imperfections

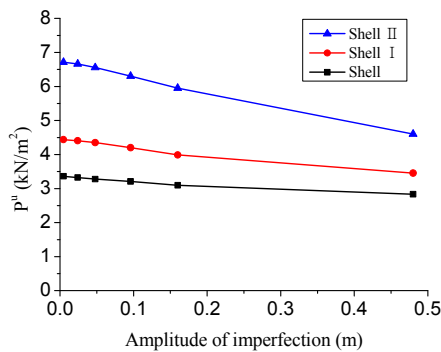


Fig. 17 Load-carrying capacities with different amplitudes of imperfection

Figs. 16 and 17 show the effect of imperfection on the load-carrying capacity of the latticed shells. As it can be seen, the load-carrying capacities of all the three types of latticed shells decrease with the increase of the imperfection magnitude. However, the sensitivity of cylindrical latticed shells is much small compared with other latticed domes analysed by Zugasti *et al.* (2012). Moreover, it must be noted that the cable-stiffened latticed shells are a bit more sensitive to the level of the imperfection.

4.5 The effect of asymmetrical load distribution

The results analyzed above were obtained from the latticed shells under uniform load. However, the structure is subjected to both the uniformly load and non-uniformly load (such as the snow load) in practical engineering, which

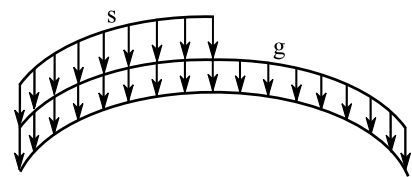


Fig. 18 Load distribution of the latticed shell

means that it is necessary to investigate the behaviour of the structure under non-uniform distributed load. Fig. 18 illustrates the load distribution of the latticed shell. The symbol g is used to denote the load distributed over the whole span uniformly, and s is used to denote the load distributed over half of the span uniformly. In this section, the ratio of s/g varies from 0 to 1 to simulate different cases. Fig. 19 shows the equilibrium paths represented by the total load versus the displacement with s/g varying. The total load is defined as all the loads applied to the nodes of the latticed shell. As it can be seen, the load-carrying capacities and structural stiffness of all the latticed shells have been decreased by the asymmetrical loads. However, it should be noted that the decrease rate of the structural stiffness of the ordinary unstiffened latticed shell is much higher than those of the cable-stiffened latticed shells (Shell I and Shell II). In other words, the structural stiffness becomes less sensitive to the asymmetrical load with the introduction of the cable-stiffened systems.

4.6 The effect of boundary conditions

For all the FE analyses discussed above, the supports of

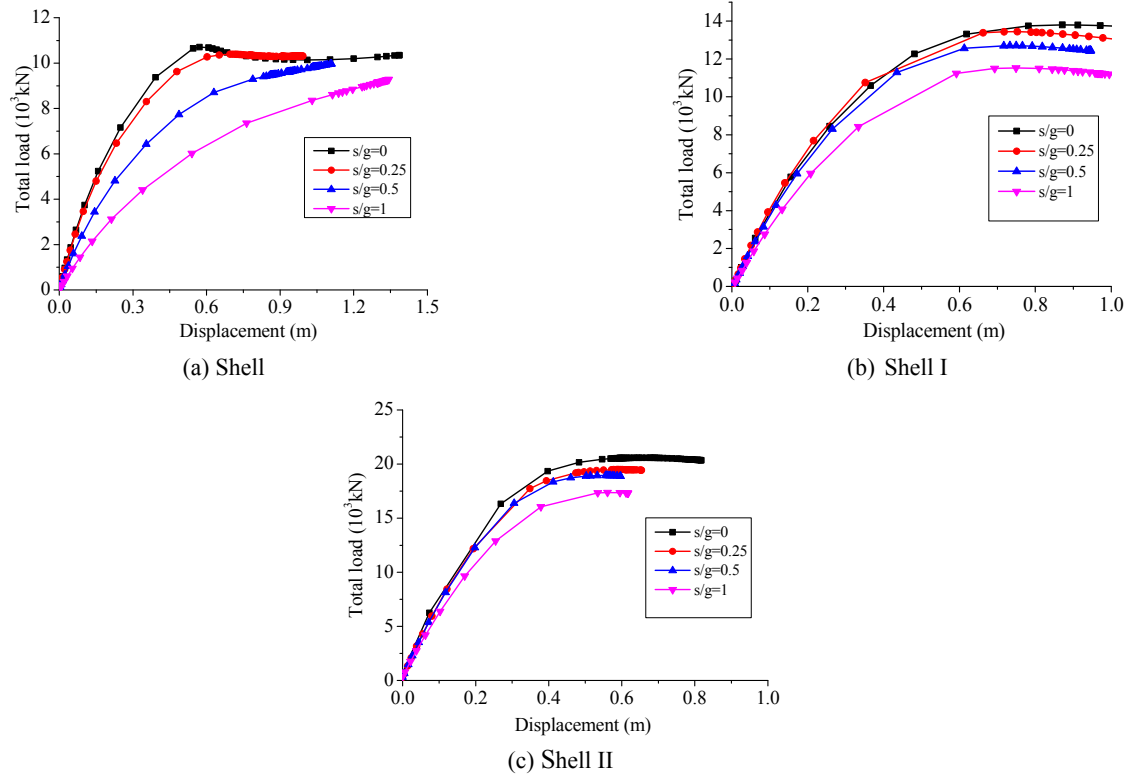


Fig. 19 Equilibrium paths with s/g varying

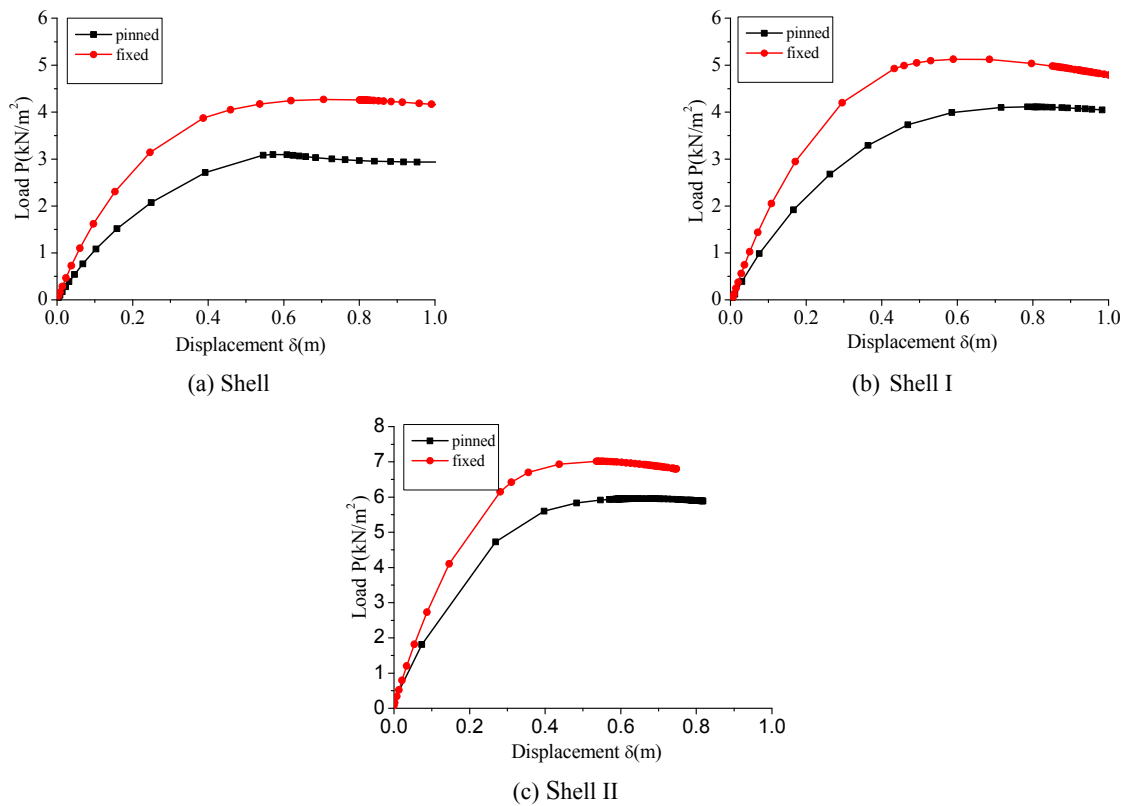


Fig. 20 Equilibrium paths with different boundary conditions

all the latticed shells are regarded as pinned on their four edges. This section aims to investigate the load-carrying capacities of the latticed shells with different boundary

conditions. Fig. 20 shows the equilibrium paths of the latticed shells with different boundary conditions. Obviously, the load-carrying capacities of all the latticed

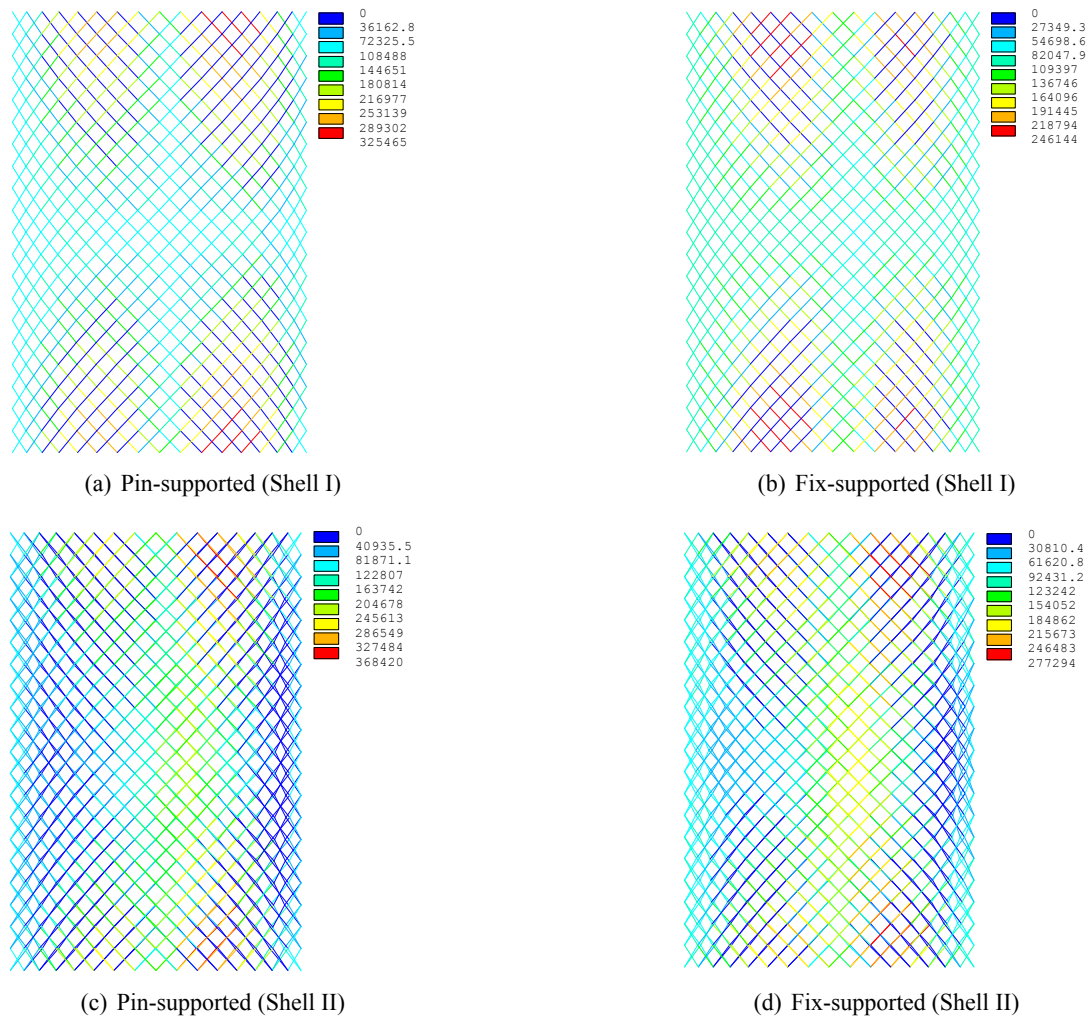


Fig. 21 Axial forces in cables of different latticed shells

Table 2 Maximum plastic strains of different latticed shells

| Boundary conditions | Shell | Shell I | Shell II |
|---------------------|--------|---------|----------|
| Pin-supported | 0.0056 | 0.0076 | 0.0229 |
| Fix-supported | 0.0220 | 0.0236 | 0.0412 |

shells have been enhanced with the boundary condition changed from pinned to fixed. In other words, enough attention must be paid to the boundary condition while designing these types of structures. Table 2 presents the maximum plastic strains of different latticed shells near boundaries. It can be observed that the plastic strain of fix-supported shells is greater than those of pin-supported shells, implying that the bending moment corresponds to the fix-supported shell is much greater.

Fig. 21 illustrates the axial forces in cables of Shell I and Shell II under different boundary conditions. It can be observed that the distributions of slacked cables in cable-stiffened latticed shells under different boundary conditions are similar, however, the axial forces of cables in the latticed shell supported by pinned supports are larger than those corresponds to fixed supports. It is understandable that the deflections, which correspond to the load-carrying

capacity, of the latticed shells supported by pinned supports are much larger (see Fig. 20) owing to the different boundary stiffness. Thus, the number of slacked cables is larger when the boundary condition is pinned supports; similarly, the axial forces of the tensioned cables are larger if the latticed shell is pin-supported.

5. Conclusions

This article investigated the stability behaviour of the cable-stiffened cylindrical latticed shells with different types of cable layouts. The most notable findings can be summarised as below:

- The lowest linear buckling mode of cable-stiffened cylindrical latticed shell is different from that of the ordinary one. The front elevation of the buckling mode shape change from two half sine waves to three half sine waves by the cable-stiffened system, implying that the structure stiffness has been improved. Moreover, the critical load of cylindrical latticed shell is increased as well due to the cable-stiffened system.
- Both the load-carrying capacity and stiffness of the

ordinary cylindrical latticed shell are improved by the cable-stiffened system. The load-carrying capacity of Shell II is higher than that of Shell I. Because only the in-plane shear stiffness is stiffened in Shell I, while both the in-plane shear stiffness and the out-of-plane bending stiffness are strengthened in Shell II.

- It has been demonstrated through the analyses that both the increase of the cross-sectional of the cables and pretension in cables would lead to the improvement in load-carrying capacity. However, the same increment of cross-section and pretension would lead to different increment in load-carrying capacity for the two types of cable-stiffened latticed shells, the increase rate of Shell II is much higher than that of Shell I.
- The types of joints analysed in this paper have negligible effect on the load-carrying capacities of the cable-stiffened latticed shells, while the effect on the corresponding ordinary single-layer latticed shells should be taken into account. In other words, the introduction of the cables decreases the sensitivity of the single-layer latticed shells to the types of joints, which indicates that it is possible to adopt the scissor-type joint for cable-stiffened cylindrical latticed shell in engineering application without decreasing the load-carrying capacity.
- The load-carrying capacities of the cylindrical latticed shells are decreased by the initial imperfection, especially when the magnitude of imperfection exceeds $B/300$ (B is the span of the shell). Thus, initial imperfection must be taken into account in designing these types of structure.
- The load-carrying capacities and the structural stiffness of the cable-stiffened latticed shells (Shell I and Shell II) have been decreased by the asymmetrical load. However, the decrease rate of the structural stiffness of the ordinary unstiffened latticed shell is much higher than those of the cable-stiffened latticed shells (Shell I and Shell II). In other words, the structural stiffness becomes less sensitive to the asymmetrical load with the introduction of the cable-stiffened systems.
- The boundary conditions have considerable effect on the load-carrying capacities of the cylindrical latticed shells, which means it is necessary to pay enough attention to the boundary condition while designing or constructing the structure.

Acknowledgments

This work was funded by the National Natural Science Foundation of China through the research project: 51178331.

References

Alan, H. (1997), *The Art of Structural Engineering*, Edition Axel Menges, Stuttgart, Germany.
ANSYS (2013), Release 15.0 document for ANSYS.

- Bulenda, T.h. and Knippers, J. (2001), "Stability of grid shells", *Comput. Struct.*, **79**(12), 1161-1174.
- Cai, J.G., Zhou, Y., Xu, Y.X. and Feng, J. (2013), "Non-linear stability analysis of a hybrid barrel vault roof", *Steel Compos. Struct., Int. J.*, **14**(6), 571-586.
- Cai, J.G., Jiang, C., Deng, X.W., Feng, J. and Xu, Y.X. (2015), "Static analysis of a radially retractable hybrid grid shell in the closed position", *Steel Compos. Struct., Int. J.*, **18**(6), 1391-1404.
- EN 1993-1-6 (2007), Design of steel structures-Part 1-6: Strength and stability of shell structures; European Committee for Standardization.
- Feng, R.Q., Ye, J.H. and Yao, B. (2012), "Evaluation of the buckling load of an Elliptic Paraboloid cable-braced grid shell using the continuum analogy", *J. Eng. Mech.*, **138**(2), 1468-1478.
- Feng, R.Q., Yao, B. and Ye, J.H. (2013), "Stability of lamella cylinder cable-braced grid shells", *J. Constr. Steel Res.*, **88**, 220-230.
- Han, Q.H., Liu, Y.M. and Xu, Y. (2016), "Stiffness characteristics of joints and influence on the stability of single-layer latticed domes", *Thin-Wall. Struct.*, **107**, 514-525.
- Jiang, Z.R., Shi, K.R., Gao, X.N. and Chen, Q.J. (2013), "Analysis of nonlinear buckling of a long-span elliptic paraboloid suspended dome structure", *Adv. Mater. Res.*, **639-640**, 191-197.
- Kato, S., Mutoh, I. and Shomura, M. (1994), "Effect of joint rigidity on buckling strength of single layer lattice domes", *Bull. Int. Assoc. Shell Spatial Struct.*, **35**(2), 101-109.
- Li, P.C., Wu, M.E. and Xing, P.J. (2014), "Novel cable-stiffened single-layer latticed shells and their stabilities", *J. Constr. Steel Res.*, **92**, 114-121.
- López, A., Puente, I. and Serna, M.A. (2006), "Direct evaluation of the buckling loads of semi-rigidly jointed single-layer latticed domes under symmetric loading", *Eng. Struct.*, **29**(1), 101-109.
- Mohammadi, M., Abedi, K. and Taghizadieh, N. (2012), "Stability analysis of single-layer barrel vault space structures", *Int. J. Space Struct.*, **27**(4), 203-218.
- Ramalingam, R. and Jayachandran, S.A. (2015), "Postbuckling behaviour of flexibly connected single layer steel domes", *J. Constr. Steel Res.*, **114**, 136-145.
- Schlaich, J. and Schober, H. (1996), "Glass-covered grid-shells", *Struct. Eng. Int.*, **6**(2), 88-90.
- Schlaich, J. and Schober, H. (1997), "Glass Roof for the Hippo House at the Berlin Zoo", *Struct. Eng. Int.*, **7**(4), 252-254.
- Technical specification for space frame structures (2010), Beijing, China. [In Chinese]
- Umezawa, R., Hiraoka, S., Takahashi, K., Sunahara, H. and Kurosawa, T. (2003), "On design of Kumagaya Dome of a super large single layer reticular dome with membrane roof recently constructed in Japan", *Proceedings of IASS-APCS 2003*, Taipei, Taiwan, September.
- Wen, M., Wang, X.F. and Deng, Z.C. (2011), "The study on performance of single-layer cylinder shells with semi-rigid bolt-ball joints", *Adv. Mater. Res.*, **243-249**, 222-228.
- Wu, H. and Wu, M.E. (2012), "Approximate evaluation of the buckling load of cable-stiffened two-way grid shell", *Proceedings of the 14th Spatial Structures Symposium*, Fuzhou, China, November. [In Chinese]
- Yamashita, T. and Kato, S. (2001), "Elastic buckling characteristics of two-way grid shells of single layer and its application in design to evaluate the non-linear behavior and ultimate strength", *J. Constr. Steel Res.*, **57**(12), 1289-1308.
- Yamada, S, Akiko, T., Yoshiyuki, T. and Kazutoshi, T. (2001), "Imperfection-sensitive overall buckling of single-layer lattice domes", *J. Eng. Mech.*, **127**(4), 382-386.
- Zhang, Z. and Fujimoto, M. (2010), "Effect of tension member on buckling and strength behavior of single layer two-way grid

- cylindrical shell roof”, *Proceedings of the IASS 2010 Symposium*, Shanghai, China, November, pp. 432-434.
- Zugasti, A.A., Lopez-Arancibia, A. and Puente, I. (2012), “Influence of geometrical and structural parameters on the behaviour of squared plan-form single-layer structures”, *J. Constr. Steel Res.*, **72**, 219-226.

DL